Korean J. Chem. Eng., 39(10), 2691-2701 (2022)
DOI: 10.1007/s11814-022-1155-7

pISSN: 0256-1115
eISSN: 1975-7220

Novel NO removal using combined sodium erythorbate and $Fe^{II}EDTA$ system

Lirong Zhong, Feiqiang He†, Beibei Dong, and Jianhua Ding†

Jiangxi Key Laboratory for Mass Spectrometry and Instrumentation, East China University of Technology, Nanchang 330013, P. R. China

(*Received 6 January 2022 • Revised 1 April 2022 • Accepted 24 April 2022*)

Abstract−To solve the difficulty of easy oxidation of $Fe^{II}EDTA$ in nitric oxide removal, $Fe^{II}EDTA$ combined with sodium erythorbate (SE) was employed for nitric oxide absorption. SE quickly reduced $Fe^{III}EDTA$ to $Fe^{II}EDTA$ and maintained $Fe^{II}EDTA$ activity for a long time in the air. The influences of various operating parameters such as $Fe^{II}EDTA$ concentration, SE concentration, original pH value and temperature on NO removal in the bubbling device were examined preliminarily. The results reveal that the SE significantly enhanced nitric oxide absorption with $Fe^{II}EDTA$. Nitric oxide absorption efficiency increased with the increase in the concentration of absorbent components or the decrease in temperature. Weak alkalinity (about pH 8.0) is beneficial to NO absorption. Besides, the NO removal efficiency continually decreased as the NO or O_2 concentration increased, while the NO removal efficiency increased first and then decreased as the SO_2 concentration increased. However, pH and temperature hardly affected nitric oxide absorption efficiency at $Fe^{II}EDTA$ with high concentration. Finally, the kinetic studies demonstrated that NO absorption by mixed $Fe^{II}EDTA$ and SE was more effective in reducing total mass transfer resistance and enlarging the NO flux compared with the normal $Fe^{II}EDTA$ approach. The absorption process was controlled by the liquid film.

Keywords: Nitric Oxide, Sodium Erythorbate, $Fe^{II}EDTA$, Removal

INTRODUCTION

The terrible air pollution incidents that have occurred in developing countries are mainly attributed to the chemical smog produced by the photocatalysis of nitric oxides (NOx) [1-3]. Selective catalytic reduction (SCR) using NH_3 at 300-500 °C by the precious metal catalyst is supposed to be the best available NOx control technology, in which nitric oxide can be transformed into nontoxic N_2 with NH_3 [4,5]. However, the operating and preservation of SCR are costly in the median and small industrial boilers and furnaces [6,7]. Developing an efficient and economical method for nitric oxide (NO) removal is one of the hot topics in the field of air pollution control.

Complex denitrification is one of the desirable methods for nitric oxide removal [8-11] Among them, the $Fe^{II}EDTA$ complex has been a well-studied absorbent since the 1970s owing to the fast complexing ability on nitric oxide [12]. $Fe^{II}EDTA$ can quickly capture nitric oxide to produce ferrous-nitrosyl complex $Fe^{II}EDTA$-NO, and the equilibrium constant reached was $10^7\ M^{-1}$ (Eq. (1)) [13]. However, a fatal flaw of $Fe^{II}EDTA$ is that it can be easily oxidized to produce inanimate $Fe^{III}EDTA$ (Eq. (2)) [14].

$$Fe(II)EDTA^{2-} + NO(L) \leftrightarrow Fe(II)EDTA-NO^{2-} \quad (1)$$

$$4Fe(II)EDTA^{2-} + O_2 + 4H^+ \rightarrow 4Fe(III)EDTA^- + 2H_2O \quad (2)$$

Currently, the research on nitric oxide absorption by $Fe^{II}EDTA$ focuses on the inhibition of $Fe^{II}EDTA$ oxidation or $Fe^{II}EDTA$ regeneration by appropriate additives. For example, Ma et al. [15] added sulfite into $Fe^{II}EDTA$ solution to utilize its reducibility on $Fe^{III}EDTA$ for improving NO removal, revealing that the NO removal efficiency exceeded 80% within 8 min under optimum conditions. Long et al. [16] combined a $Fe^{II}EDTA$ solution with the catalyzed regeneration by activated carbon for NO removal. The results demonstrated that the nitric oxide removal efficiency was maintained at a high level for a long time. Additionally, selenium was introduced into the SO_3^{2-}/$Fe^{III}EDTA$ system as a catalyst for $Fe^{III}EDTA$ transformation, and the $Fe^{III}EDTA$ transformation rate was only 47.6% [17]. Since sulfite and selenium are weak in $Fe^{III}EDTA$ reduction, it is difficult to maintain a high NO absorption efficiency for a long time. Therefore, Ma et al. [18] employed reducing metal powders such as Fe to improve NO removal efficiency with $Fe^{II}EDTA$ solution. They verified that the NOx removal efficiency was completely recovered after regeneration, filtration, and simple pH adjustment. The other reductive metal powder, such as zinc, manganese, and aluminum powder, can quickly reduce not only $Fe^{III}EDTA$ but also $Fe^{II}EDTA$-NO. Nonetheless, these reductive metal powders with strong reduction ability are unstable and easily oxidized by O_2 and lose activity, and hardly keep the stability of $Fe^{II}EDTA$ for a long time in the air. In addition, microorganism combined with $Fe^{II}EDTA$ was used for denitrification, in which microbial strains reduced $Fe^{III}EDTA$ and $Fe^{II}EDTA$-NO with glucose, organic carbon source and even $Fe^{II}EDTA$ itself as electron donors, and the complex NO was reduced and decomposed into non-toxic and pollution-free N_2. Finally, $Fe^{II}EDTA$ was obtained again to continue to absorb NO. Dong et al. [19] adopted single strain *Pamcoccus denitrification* ZGL simultaneously to reduce $Fe^{II}EDTA$-NO and $Fe^{III}EDTA$, finding that $Fe^{II}EDTA$-NO and $Fe^{III}EDTA$ were reduced by 87% and 17.55% within 3 h, respectively. However, complicated conditions involving bacteria culture, the harmful influence of sul-

†To whom correspondence should be addressed.
E-mail: he_feiqiang@ecit.cn, dingjianh2004@126.com

fur compounds from flue gas, and the costs of technological operation, limit the further development of microorganisms on $Fe^{II}EDTA$ denitrification. Therefore, finding a stable, efficient, and low-cost reductant of $Fe^{III}EDTA$ is of great significance.

Besides reducing $Fe^{III}EDTA$, inhibiting the oxidation of $Fe^{II}EDTA$ is also essential to maintaining the stability of $Fe^{II}EDTA$ in the denitrification process. Thus, the material will maintain the stability of $Fe^{II}EDTA$ if it has strong oxidation resistance and reducibility. In our previous published work [20], ascorbic acid (VC) was revealed to be more powerful in $Fe^{III}EDTA$ reduction and, particularly, it can keep the stability of $Fe^{II}EDTA$ for a long time in the air. NO absorption was significantly improved by $Fe^{II}EDTA$ through VC. Sodium erythorbate (SE) has similar properties to VC, as well as a strong antioxidant and reductive properties. Additionally, its price is half cheaper than VC. Therefore, combining SE with $Fe^{II}EDTA$ for NO removal would significantly ensure $Fe^{II}EDTA$ stability and improve NO removal.

This study investigated the interactions between SE and $Fe^{II}EDTA$ regarding $Fe^{III}EDTA$ or $Fe^{II}EDTA$-NO reduction and inhibition of $Fe^{II}EDTA$ oxidation by SE. Furthermore, the absorption of nitric oxide (NO) from simulated flue by the mixed SE and $Fe^{II}EDTA$ system was explored to demonstrate the unique advantages. This finding lays a foundation for industrial denitrification with a mixed $Fe^{II}EDTA$ and SE system.

EXPERIMENTAL

1. Chemicals

Sodium erythorbate (98.0%), Na_2EDTA (99.0%), $FeSO_4$ (99.0%) and other reagents used in the experiments were provided by Tianjin Kermel Chemical Reagent Co., Ltd., China. Nitrogen (99.999%), and nitric oxide (99.99%) were purchased from Nanchang Huate Gas Co., China. Air was provided by an air compressor. All reagents were analytical reagents.

2. The Relation between SE and $Fe^{II}EDTA$

The reduction of $Fe^{III}EDTA$ and inhibition of $Fe^{II}EDTA$ oxidation by SE were investigated to comprehensively explore the relation between SE and $Fe^{II}EDTA$ on NO removal. The experimental apparatus and procedures are exhibited in Text S1.

3. NO Removal by $Fe^{II}EDTA$ Combined with SE

The flow-process chart of NO removal is presented in Text S2. The system was composed of a gas simulation system, a laboratory-scale bubbling reactor system, and a gas sampling-analysis system. The absorption of NO was in the 500 mL laboratory-scale bubbling reactor. The pressure of the laboratory-scale bubbling reactor was atmospheric pressure. The concentration of NO was analyzed by a flue gas analyzer (KM950, KANE International Ltd) after being dried with anhydrous calcium chloride. NO absorption efficiency was defined as:

$$\eta_{AE}(t)=\frac{c_{in}-c_{out}}{c_{in}}\times 100\% \quad (3)$$

$$\overline{\eta}_{AE}=\frac{1}{40}\int_{2}^{40}\eta_{AE}(t)dt \quad (4)$$

where $\eta_{AE}(t)$ denotes NO absorption efficiency at time t; $\overline{\eta}_{AE}$ is average NO removal efficiency during the absorption process of 40 min; c_{in} stands for ingress nitric oxide concentration, ppm; c_{out} stands for exited nitric oxide concentration, ppm. Flue gas analyzer (KM950) was adopted to measure the NO concentration.

4. Analysis Methods

The Fe(II) concentration was measured with the o-phenanthroline colorimetry at an absorbance of 510 nm [21]. The $Fe^{II}EDTA$-NO concentration was detected using a UV/vis spectrophotometer (UV-2450, Japan Shimadzu) at an absorbance of 434 nm [22,23].

RESULTS AND DISCUSSION

1. The Relation between SE and $Fe^{II}EDTA$

Fig. 1(a) suggests that $Fe^{III}EDTA$ was reduced to $Fe^{II}EDTA$, and the reduction rate increased as the molar ratio of SE to $Fe^{III}EDTA$ increased. For example, the produced $Fe^{II}EDTA$ concentrations were 0.00116 M, 0.00199 M, 0.002 M and 0.002 M, by the mole ratio of 0.25, 0.5, 0.75 and 1, respectively. The results demonstrated that SE presented an excellent reducing ability of $Fe^{III}EDTA$. The prominent disadvantage of $Fe^{II}EDTA$ was that it was easy to be oxidized by O_2 in flue gas during the process of NO removal, resulting in a rapid decrease in NO removal efficiency. Therefore, the control of $Fe^{II}EDTA$ oxidation is a crucial step in $Fe^{II}EDTA$ denitrification [24]. Additionally, the effects of temperature on $Fe^{II}EDTA$ oxidation by SE were investigated. As observed in Fig. 1(b), the $Fe^{II}EDTA$ oxidation can be divided into two stages. At the first stage (0-120 min), $Fe^{II}EDTA$ oxidation was hardly affected, and $Fe^{II}EDTA$ concentration remained unchanged under different temperatures. In the second stage, the $Fe^{II}EDTA$ oxidation rate increased as the temperature increased. High temperature is not conducive to the inhibition of $Fe^{II}EDTA$ oxidation, because it can accelerate the molecule movement and boost $Fe^{II}EDTA$ oxidation rate through Eq. (2) with endothermic reaction [24].

The traditional approach to calculate the kinetics of $Fe^{II}EDTA$ oxidation with SE is to add excessive one of reactants during the reaction process [25]. In this study, the SE concentration during the reaction process was considered constant since it remarkably exceeded the $Fe^{II}EDTA$ concentration. At the first stage (0-120 min), $Fe^{II}EDTA$ was hardly oxidized. Thus, the second stage (120-240 min) was selected as the experimental subjects for kinetics calculation. The $Fe^{II}EDTA$ oxidation rate was expressed as Eq. (5).

$$r=-\frac{d[Fe^{II}EDTA]}{dt}=k_{obs}[Fe^{II}EDTA]^{\alpha} \quad (5)$$

where α denotes the reaction order of $Fe^{II}EDTA$; r and k_{obs} represent oxidation rate and observed rate constant, respectively; $[Fe^{II}EDTA]$ indicates the concentration of $Fe^{II}EDTA$.

The $Fe^{II}EDTA$ oxidation was assumed as 1 and then validated by experimental data. According to Eq. (5), the experimental data under various temperature are represented as a plot of $\ln[Fe^{II}EDTA]$ versus time in Fig. 1(c). It can be seen that these plots are all linear with the correlation coefficients (r^2) of 0.9623, 0.9780, 0.9964, and 0.9992 at 30, 40, 50 and 60 °C, respectively. We can also find that the $Fe^{II}EDTA$ oxidation presents pseudo-first-order on $Fe^{II}EDTA$, in which correlative coefficients (r^2) are 0.9623, 0.9780, 0.9964, and 0.9992 with 30, 40, 50, and 60 °C, respectively (Fig. 7(b)). In addi-

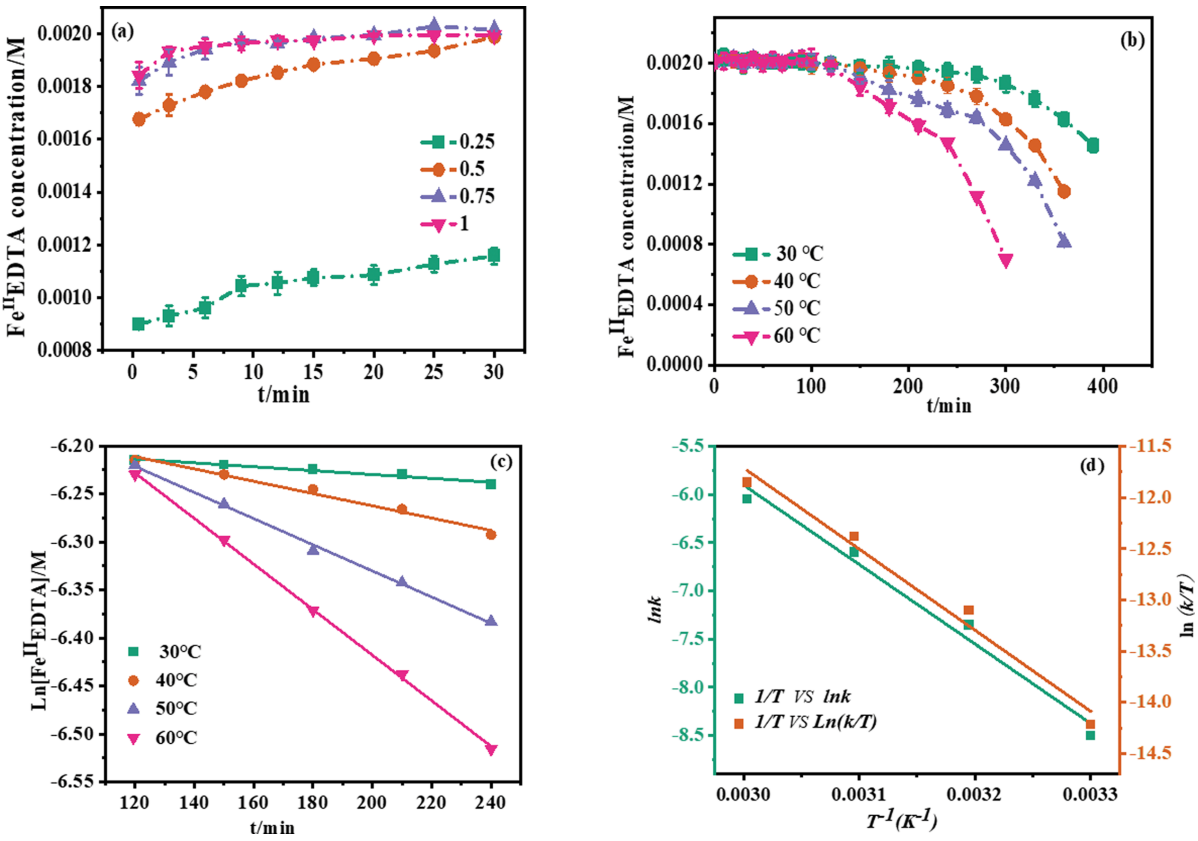

Fig. 1. (a) The effect of the molar ratio on $Fe^{III}EDTA$ reduction at pH 6.0, 30 °C, 0.002 M $Fe^{III}EDTA$. (b) The effect of temperature on inhibited oxidation at pH 6.0 with a molar ratio of SE to $Fe^{II}EDTA$ of 8. (c) The plots of ln[$Fe^{II}EDTA$] versus time (t). (d) The line chart of the Arrhenius and Eyring-Polanyi formulas.

tion, the corresponding k_{obs} obtained from the gradients of the linear plots increases as temparature rises, i.e., 2.025×10^{-4}, 6.404×10^{-4}, 1.36×10^{-3}, and 2.37×10^{-3} min^{-1}.

In addition, activation energy (E_a), activation enthalpy ($\Delta H^{\ddagger}$), activation entropy ($\Delta S^{\ddagger}$) were calculated based on Arrhenius and Eyring-Polanyi formula by Eqs. (6) and (7).

$$\ln k_{obs} = -E_a/RT + \ln(A) \quad (6)$$

$$\ln\frac{k_{obs}}{T} = -\frac{\Delta H^{\ddagger}}{R}\frac{1}{T} + \ln\frac{k_B}{h} + \frac{\Delta S^{\ddagger}}{R} \quad (7)$$

where A is pre-exponential factor, R is the universal gas constant (R=8.314 J k^{-1} mol^{-1}), T is for the absolute temperature (K), k_B is Boltzmann's constant (1.38×10^{-23} J K^{-1}), h is Planck's constant (6.63×10^{-34} J s).

Therefore, E_a is equal to (−R) multiplied by the slope of the plot about ln(k) vs (1/T) and was computed to be 68.505 kJ mol^{-1} (Fig. 1(d)). $\Delta H^{\ddagger}$ (65.827 kJ mol^{-1}) and $\Delta S^{\ddagger}$ (−97.415 J k^{-1} mol^{-1}) were calculated from the gradient and intercept of the fitted line chart of ln(k/T) versus 1/T, respectively (Fig. 1(d)). The large negative $\Delta S^{\ddagger}$ implied that the $Fe^{II}EDTA$ oxidation by SE was associative.

Table 1. Comparison of the relation between different system and $Fe^{II}EDTA$

Reference	$Fe^{II}EDTA$-NO reduction		$Fe^{III}EDTA$ reduction		$Fe^{II}EDTA$ oxidation[a]	
	Reduction efficiency (initial concentration)	Time	Reduction efficiency (initial concentration)	Time	Oxidation efficiency (initial concentration)	Time
P. denitrificans ZGL1 [19]	87% (1.45 mM)	3 h	17.5% (4.8 mM)	3 h	No work	
Na_2SO_3 [27]	No research		about 65% (10 mM)	120 min	71.65% (2 mM)	20 min
$(NH_2)_2CSO_2$ [28]	91.4% (2 mM)	30 min	100% (2 mM)	30 min	56.2% (2 mM)	20 min
$Na_2S_2O_4$ [29]	69.4% (1.41 mM)	30 min	99.5% (50 mM)	3 min	76.8% (2 mM)	50 min
Zn [30]	97.5% (10 mM)	20 min	98.12% (10 mM)	20 min	88.9% (2 mM)	100 min
VC [20]	No work		96.5% (2 mM)	3 min	13% (2 mM)	390 min
SE	No work		96.4% (2 mM)	3 min	27% (2 mM)	390 min

[a]The data were obtained by our research group.

In addition, to highlight the advantages of SE in the $Fe^{II}EDTA$ inhibition oxidation, other $Fe^{II}EDTA$ systems (Na_2SO_3, $(NH_2)_2CSO_2$, $Na_2S_2O_4$, Zn, and VC) on $Fe^{II}EDTA$ inhibition oxidation under the same experimental conditions were also investigated. From Table 1, the result showed that SE presented fantastic inhibition performance, and the $Fe^{II}EDTA$ oxidation efficiency was less than 30% within 390 min. Therefore, SE has high efficiency in reducing $Fe^{III}EDTA$ and inhibiting $Fe^{II}EDTA$ oxidation. This was because the dienol group in SE molecule had strong reducibility, leading to $Fe^{III}EDTA$ reduction [26]. In addition, under the strong reducing effect, SE can react with O_2^-, HOO^- and OH^- quickly to produce dehydroisoascorbic acid, and eliminate the toxicity of harmful oxygen free radicals, and inhibit the oxidation of $Fe^{II}EDTA$, presenting strong antioxidant activity. Therefore, compared with other systems (Table 1), SE has high efficiency in reducing $Fe^{III}EDTA$ and inhibiting $Fe^{II}EDTA$ oxidation, which lays a theoretical foundation for the efficient removal of NO by $Fe^{II}EDTA$ combined with SE.

2. Effect of SE Concentration on Nitric Oxide Absorption

The influence of SE concentration on nitric oxide absorption efficiency is illustrated in Fig. 2(a). NO removal efficiency η_{AE} with only $Fe^{II}EDTA$ decreased rapidly with time and was less than 40% after 16 min. Similarly, η_{AE} with 0.0025 M SE was kept at approximately 70% for 20 min and then suddenly decreased to 55%. Besides, η_{AE} started to slowly decrease with time when 0.005 M SE was added into the $Fe^{II}EDTA$ solution. Particularly, η_{AE} at SE greater than 0.01 M was maintained at over 86% during the whole NO removal process. These results suggest that SE played an intense positive role in promoting nitric oxide removal by $Fe^{II}EDTA$. The enhancement effect was more significant at high SE concentrations.

The specific reasons are analyzed as follows. First, the nitric oxide capture reaction through Eq. (1) plays a decisive role in nitric oxide absorption, in which the concentration of $Fe^{II}EDTA$ can directly impact the NO removal efficiency at the same temperature and pH value. Thus, the $Fe^{II}EDTA$ concentration was analyzed. Nevertheless, it is difficult to measure $Fe^{II}EDTA$ concentration directly. Since total Fe(II) from absorption liquid consists of $Fe^{II}EDTA$ and $Fe^{II}EDTA$-NO, $Fe^{II}EDTA$ concentration was obtained from the difference between total Fe(II) and $Fe^{II}EDTA$-NO concentration. In Fig. 2(b), $Fe^{II}EDTA$ tended to be oxidized at a lower concentration of SE. For example, the free $Fe^{II}EDTA$ concentration quickly decreased with time when SE concentration was lower than 0.0025 M. $Fe^{II}EDTA$ oxidation through Eq. (2) started to slowly govern the process, and the role of Eq. (1) was weakened. There was no $Fe^{II}EDTA$ in the solution at the end. Hence, the NO removal efficiency at below 0.0025 M SE rapidly decreased with time. Concerning the SE concentration with 0.005 M, the free $Fe^{II}EDTA$ concentration slowly decreased with time, contributing to the slow decrease in the NO removal efficiency. Regarding SE with a concentration greater than 0.01 M, Fe(II) concentration was kept at 0.004 M during the whole NO removal process, indicating that all Fe(II) was not oxidized, mainly including free $Fe^{II}EDTA$ and produced $Fe^{II}EDTA$-NO. Therefore, nitric oxide removal primarily depended on the NO capture reaction through Eq. (1), in which reaction rate was given by $r=k C_{Fe^{II}EDTA} C_{NO}$ (k denotes reaction rate; $C_{Fe^{II}EDTA}$ and C_{NO} represent $Fe^{II}EDTA$ and nitric oxide concentrations, respectively). The changing trend of free $Fe^{II}EDTA$ concentration at 0.01 M and 0.02 M was consistent. Their concentrations were higher than 0.002 M and were ample during the whole absorption process. With the same temperature, nitric oxide inlet concentration, and pH values, their reaction rates k were close and up to 10^8 M^{-1}. Consequently, their NO removal efficiencies were deservedly close and maintained at about 90% during the whole nitric oxide removal process.

Finally, the NO average removal efficiency $\overline{\eta}_{AE}$ was analyzed and increased with the increasing SE concentration. For example, $\overline{\eta}_{AE}$ significantly increased from 37.25% to 92.37% as SE concentration increased from 0 M to 0.02 M. This was positively correlated with the $Fe^{II}EDTA$-NO concentration. Their relation was confirmed by the change in the color of the absorption liquid. It is widely reported that $Fe^{II}EDTA$-NO was black-brown and became darker at higher $Fe^{II}EDTA$-NO concentrations [31,32]. $\overline{\eta}_{AE}$ was consistent with color change. According to the above analysis, the darker color indicates that more NO is trapped and $\overline{\eta}_{AE}$ is higher, because SE does not react with $Fe^{II}EDTA$-NO. The color transform further indicates that nitric oxide removal is directly governed by Eq. (1).

3. Effect of $Fe^{II}EDTA$ Concentration on Nitric Oxide Absorption

Considering that $Fe^{II}EDTA$ is the most critical active ingredient capturing nitric oxide, it is imperative to explore the influence of

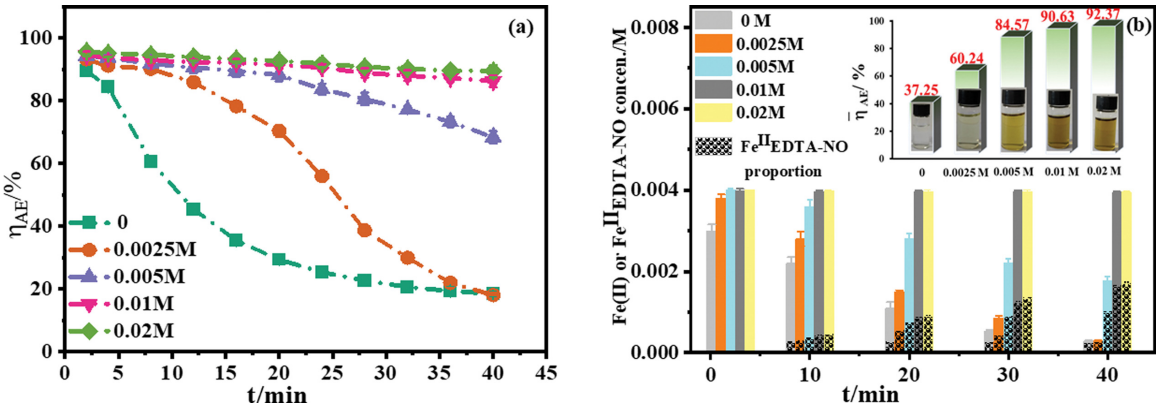

Fig. 2. (a) NO removal efficiency η_{AE} under different SE concentrations. (b) The changes of Fe(II) and $Fe^{II}EDTA$-NO concentrations, and $\overline{\eta}_{AE}$ with the color under different SE concentrations (experimental parameters: temperature, 25 °C; pH value 8.0; 9% (v/v) O_2; 0.004 M $Fe^{II}EDTA$).

$Fe^{II}EDTA$ concentration on nitric oxide absorption. Fig. 3(a) implies that SE had no absorptive capacity for nitric oxide, in which η_{AE} rapidly dropped to below 10%. The NO removal efficiency rapidly increased after SE was added to $Fe^{II}EDTA$, and the average removal efficiencies were 75.83%, 84.57%, 94.39%, and 97.96%, respectively, with initial $Fe^{II}EDTA$ of 0.002 M, 0.004 M, 0.008 M, and 0.016 M (Fig. 3(b)).

NO removal efficiency at 0.002 M $Fe^{II}EDTA$ decreased with time and finally dropped to 42.38%. This suggests that NO was hardly absorbed in the later stage of removal. The Fe(II) and $Fe^{II}EDTA$-NO concentrations were close, indicating few free $Fe^{II}EDTA$ in the solution. Therefore, η_{AE} with an initial $Fe^{II}EDTA$ of 0.002 M was very low at the end of the process, and η_{AE} with over 0.004 M $Fe^{II}EDTA$ dropped slowly with time. For example, the η_{AE} at 0.008 and 0.016 M $Fe^{II}EDTA$ were still 91.13% and 95.65% in 40 min, respectively. In this study, the corresponding differences between Fe(II) and $Fe^{II}EDTA$-NO were relatively large, reflecting that the free $Fe^{II}EDTA$ was ample. Therefore, their reaction rates k were also close and up to $10^8\ M^{-1}$ with the same temperature, nitric oxide inlet concentration, and pH, according to the complex reaction of nitric oxide via Eq. (1). Thus, their NO removal efficiencies were deservedly close and maintained at about 90% during the whole NO absorption process.

4. Effect of Temperature on Nitric Oxide Absorption

Temperature plays an essential role in gas-liquid mass transfer controlled by the diffuseness, dissolving, and reaction characteristics of chemical compounds in absorbents. The influence of temperature on nitric oxide absorption was investigated by changing the temperature from 25 to 45 °C. The effect of temperature depended on the initial concentration of $Fe^{II}EDTA$. The influence of temperature is relatively weak at an initial 0.016 M $Fe^{II}EDTA$. η_{AE} at five different temperatures was kept at over 84% during the whole removal process (Fig. 4(a)). $\overline{\eta}_{AE}$ were 97.96%, 97.14%, 95.01%, 93.44%, and 92.71%, respectively, at the temperature of 25 °C, 30 °C, 35 °C, 40 °C, and 45 °C (Fig. 4(b)).

As demonstrated in Fig. 4(b), the Fe(II) concentration was much higher than that of $Fe^{II}EDTA$-NO during the absorption process under five different temperatures; the differences between Fe(II) and $Fe^{II}EDTA$-NO concentrations in 40 min were still 0.00385 M, 0.00337, 0.00313, 0.00314, and 0.00144, respectively, at the tempera-

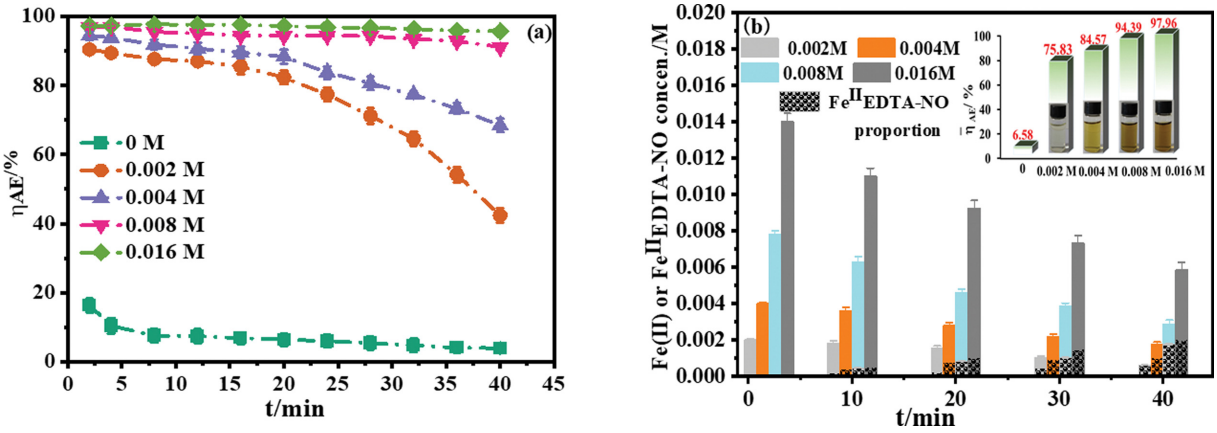

Fig. 3. (a) Nitric oxide removal efficiency η_{AE} under different $Fe^{II}EDTA$ concentrations. (b) The changes of Fe(II) and $Fe^{II}EDTA$-NO concentrations, and $\overline{\eta}_{AE}$ with the color under different $Fe^{II}EDTA$ concentrations (Experimental parameters: Temperature, 25 °C; pH value, 8.0; oxygen concentration, 9% (v/v); SE concentration, 0.005 M).

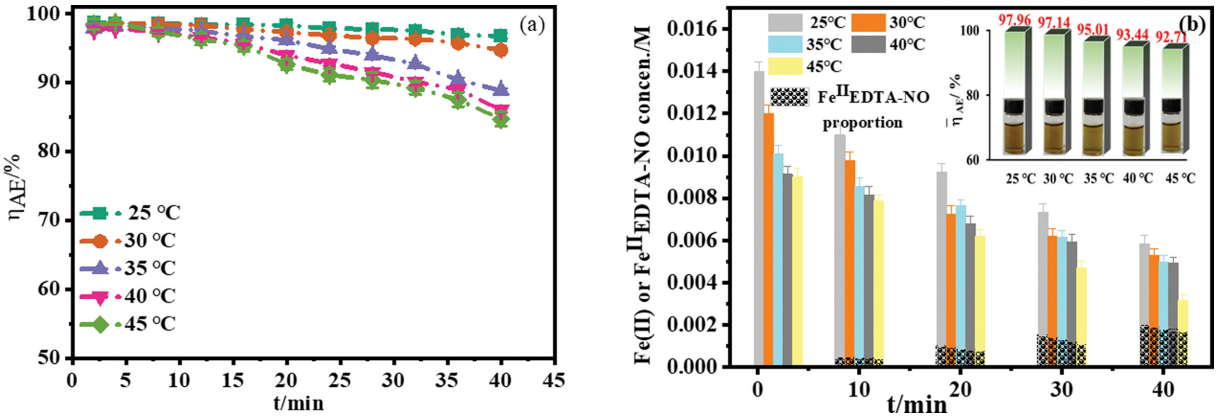

Fig. 4. (a) NO removal efficiency η_{AE} under different temperatures with time at 0.016 M $Fe^{II}EDTA$. (b) The changes of Fe(II) and $Fe^{II}EDTA$-NO concentrations, and $\overline{\eta}_{AE}$ with the color under different temperature (Experimental parameters: pH value, 8.0; oxygen concentration, 9% (v/v); SE concentration, 0.005 M).

ture of 25 °C, 30 °C, 35 °C, 40 °C, and 45 °C. This revealed sufficient free $Fe^{II}EDTA$ in the solution in the whole process. Thus, η_{AE} was mainly determined by Eq. (1). The forward reaction rate constant and equilibrium constant of NO removal by $Fe^{II}EDTA$ were extremely large even at high temperatures [33] [34]. They are about 3.3×10^{7} M^{-1} s^{-1}-1.7×10^{8} M^{-1} s^{-1}, and 1.2×10^{5} M^{-1}-3.1×10^{6} M^{-1}, respectively in 25 °C-60 °C. Therefore, NO was almost completely removed even at a low concentration of free $Fe^{II}EDTA$, and the NO removal efficiency was maintained at above 84% in the whole absorption process.

The temperature had a significant impact on nitric oxide removal at initial 0.004 M $Fe^{II}EDTA$. $\overline{\eta}_{AE}$ was 84.57%, 82.96%, 80.08%, 75.42%, and 64.82%, respectively, at 25 °C, 30 °C, 35 °C, 40 °C, and 45 °C (Fig. 5(b)). Therefore, low temperature is beneficial to nitric oxide removal by mixed absorbents.

Fig. 5(b) implies that in the first 20 min, there was sufficient free $Fe^{II}EDTA$, and the NO removal efficiencies were all about 80% at five different temperatures (Fig. 5(a)). In the second 20 min, η_{AE} decreased more significantly with time at higher temperatures (Fig. 5(a)). For example, NO was hardly absorbed as η_{AE} decreased sharply from 77.56% to 10.25% at 45 °C in the second 20 min because the decreasing rate of Fe(II) concentration increased with increasing temperature. Besides, the high temperature decreased the solubility of nitric oxide in solution, causing the decrease in η_{AE} [24].

Therefore, nitric oxide absorption should be performed at low temperatures as far as possible. Nonetheless, the temperature of the flue gas from the factory is usually higher than 300 °C. With the purpose of applying this system better in industry, high-temperature flue gas before absorption is generally cooled by water, vaporization, or spray.

5. Influence of pH on Nitric Oxide Removal

Previous reports [35] suggest that the NO removal efficiency is closely related to the pH value of the absorption solution. The effect of pH was studied by changing pH from 4.2 to 10.2. Fig. 6(a) reveals that η_{AE} at various pH values all decreased with time at an initial 0.004 M $Fe^{II}EDTA$, and the decrease rate slowed with pH 4.2-8.0. The η_{AE} decrease rate began to accelerate again once the pH exceeded 8.0. The NO average removal efficiency increased and then

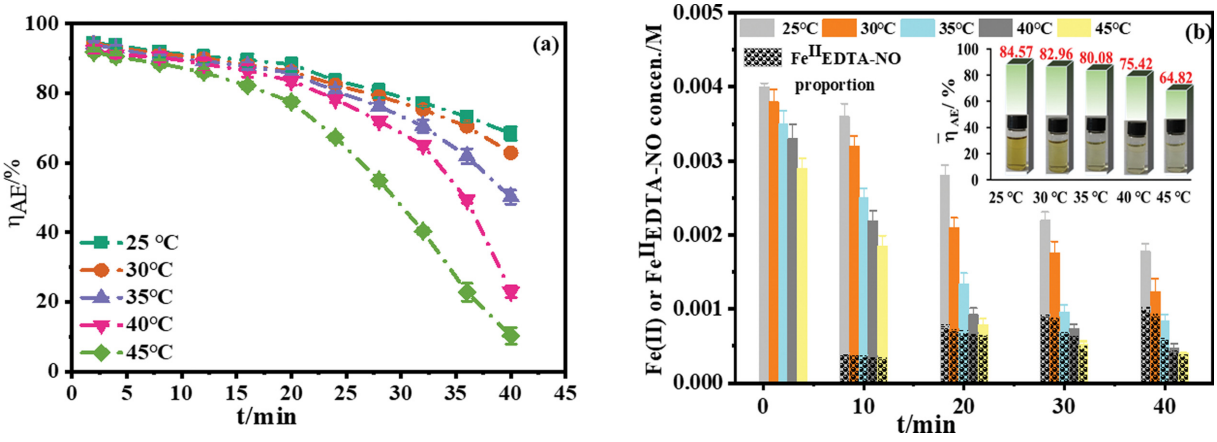

Fig. 5. (a) η_{AE} under different temperature with time at 0.004 M $Fe^{II}EDTA$. (b) The changes of Fe(II) and $Fe^{II}EDTA$-NO concentrations, and $\overline{\eta}_{AE}$ with the color under different temperatures. (Experimental parameters: pH value, 8.0; oxygen concentration, 9% (v/v); SE concentration, 0.005 M).

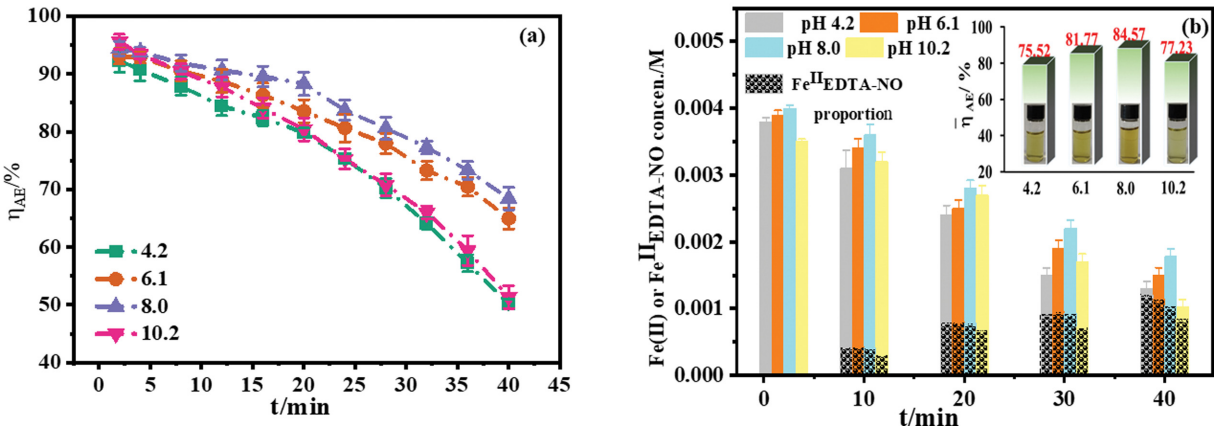

Fig. 6. (a) NO removal efficiency η_{AE} under different pH values with time at 0.004 M $Fe^{II}EDTA$. (b) The changes of Fe(II) and $Fe^{II}EDTA$-NO concentrations, and $\overline{\eta}_{AE}$ with the color under different pH values. (Experimental parameters: temperature, 25 °C; O_2 concentration, 9% (v/v); SE concentration, 0.005 M).

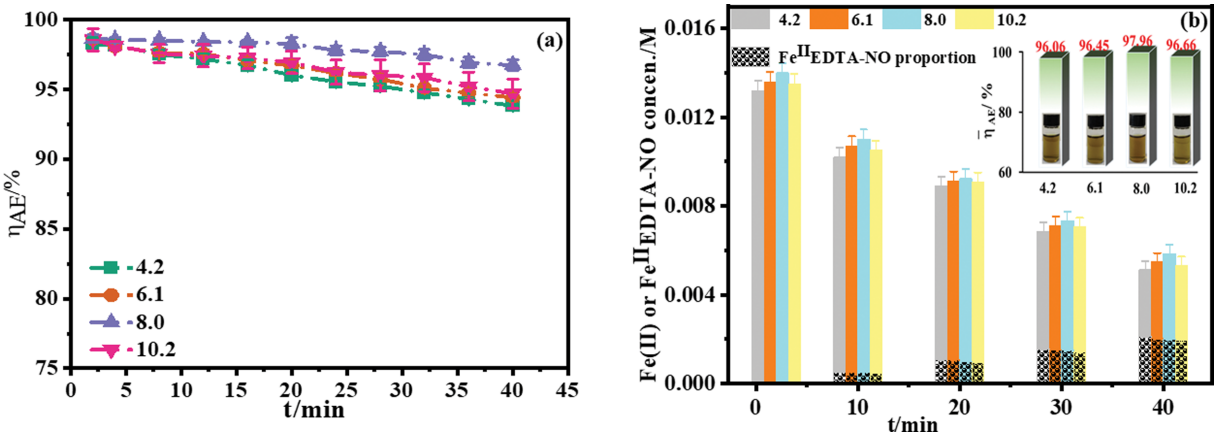

Fig. 7. (a) NO removal efficiency η_{AE} under different pH values with time at 0.016 M Fe^{II}EDTA. (b) The changes of Fe(II) and Fe^{II}EDTA-NO concentrations, and $\overline{\eta}_{AE}$ with the color under different pH values (Experimental parameters: temperature, 25 °C; O_2 concentration, 9% (v/v); SE concentration, 0.005 M).

decreased, which was 75.52% (pH 4.2), 81.77% (pH 6.1), 84.57% (pH 8.0), and 77.23% (pH 10.2). More nitric oxide was captured in the weak base in the absorption liquid, and the optimal pH was about 8.0.

As observed in Fig. 6(b), the difference between Fe(II) and Fe^{II}EDTA-NO dropped quickly under acidic (pH 4.2) and alkaline (pH 10.2) conditions, which were 0.00009 M and 0.00016 M, respectively, accounting for only 2.25% and 4% of initial Fe^{II}EDTA concentration (0.004 M). This was because Fe^{II}EDTA is easily oxidized by strong acid conditions through Eq. (2) and can easily hydrolyze and generate a precipitate in the alkaline condition through Eq. (8).

In the above discussion, NO average removal efficiency $\overline{\eta}_{AE}$ was closely related to Fe^{II}EDTA-NO concentration, reflecting the amount of NO trapped through Eq. (1). However, the NO average removal efficiency with different pH values was not consistent with Fe^{II}EDTA-NO concentration in this study. The reason was that Fe^{II}EDTA-NO was primarily composed of two parts: the direct complexation of NO with Fe^{II}EDTA and the reaction product of Fe^{II}EDTA and nitrite under the acidic condition through Eq. (9). Specifically, nitrite was formed by nitric oxide oxidizing to NO_2 and absorbing in the solution (Eqs. (10) and (11)). Hence, the final Fe^{II}EDTA-NO concentration at pH 4.2 was the highest (0.0012 M), while the NO removal efficiency was not.

$$Fe^{2+}+OH^- \rightarrow Fe(OH)_2. \quad (8)$$

$$2Fe(II)EDTA^{2-}+NO_2^-+2H^+ \rightarrow Fe(II)EDTA\text{-}NO^{2-}+Fe(III)EDTA^-+H_2O \quad (9)$$

$$NO+\frac{1}{2}O_2 \rightarrow NO_2 \quad (10)$$

$$NO+NO_2+H_2O \rightarrow 2HNO_2 \quad (11)$$

The influence of pH on nitric oxide removal at high initial Fe^{II}EDTA concentration (0.016 M) was investigated. As pH increased from 4.2 to 10.2, η_{AE} was all maintained at over 93% within 40 min (Fig. 7(a)). In Fig. 7(b), the final D-value between Fe(II) and Fe^{II}EDTA-NO was 0.00301 M (pH 4.2), 0.00344 M (pH 6.1), 0.00385 M (pH 8.0), and 0.00339 M (pH 10.2), demonstrating ample free Fe^{II}EDTA in solution within 40 min. With the same temperature and NO inlet concentration, their reaction rates k were close and up to 10^8 M^{-1}. Therefore, their η_{AE} depended on the complexation of nitric oxide through Eq. (1), whose reaction rate k reached 10^7 M^{-1} with pH 2.5-11.0 by the Weisweiler group [34].

6. Effects of the Coexistence Gases on NO Removal

Except for nitric oxide, actual flue gases in China usually contain 3-11% (v/v) oxygen and sulfur dioxide, and their concentrations always change under different technological conditions, inducing considerable effect on the absorption of nitric oxide. As observed from Fig. 8, $\overline{\eta}_{AE}$ mildly increased as sulfur dioxide concentration increased from 0 ppm to 3,000 ppm and then slightly decreased as the sulfur dioxide concentration further increased to 4,000 ppm. The increase in $\overline{\eta}_{AE}$ was associated with the formation of SO_3^{2-} after SO_2 absorption had a positive effect on the absorption of nitric oxide through Eqs. (12) and (13). Nonetheless, partial sulfur dioxide blocked the contact of nitric oxide with Fe^{II}EDTA when SO_2 concentration exceeded 4,000 ppm, contributing to an increase in mass transfer resistance between nitric oxide and liquid. As a result, $\overline{\eta}_{AE}$ would decrease.

$$2Fe(II)EDTA\text{-}NO^{2-}+SO_3^{2-} \rightarrow 2Fe(II)EDTA^{2-}+SO_3(NO)_2^{2-} \rightarrow 2Fe(III)EDTA^-+N_2O_2^{2-}+SO_3^{2-} \quad (12)$$

$$2Fe(III)EDTA^-+2SO_3^{2-} \rightarrow 2Fe(II)EDTA^{2-}+S_2O_6^{2-} \quad (13)$$

Fig. 8 reveals that low oxygen concentration is beneficial to nitric oxide removal. η_{AE} decreased as the O_2 concentration increased, and it was 92.3%, 89.96%, 87.75%, 84.57%, and 75.38%, corresponding to 3% (v/v), 5% (v/v), 7% (v/v), 9% (v/v), and 11% (v/v), respectively. This was because the Fe(II) oxidation rate increased with the increasing oxygen concentration through Eq. (2).

In Fig. 8, the denitrification efficiency decreased from 87.78% to 77.45% as the NO concentration increased from 300 to 700 ppm, which was interpreted by the decrease in the molar ratio of the complexing agent Fe^{II}EDTA to NO.

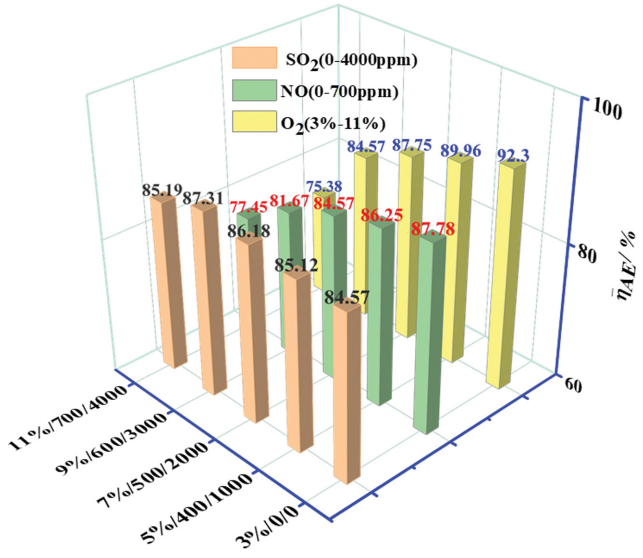

Fig. 8. The effect of coexistence gases on NO removal. Temperature, 25 °C; pH, 8.0; $Fe^{II}EDTA$, 0.004 M; SE, 0.005 M; notably, 9% (v/v) O_2 was used to investigate the effect of NO and SO_2.

7. Response Surface Methodology (RSM) Analysis

The experimental design for RSM analysis is shown in Text S3. The NO removal efficiency was measured by the different experimental conditions given by the system Design-Expert statistical software to investigate the influence imposed with the four selected variables on NO absorption efficiency. Table S1 shows the absorption efficiency of nitric oxide under various parameter values.

The NO removal efficiency was measured by the different experimental conditions given by the system Design-Expert statistical software to investigate the influence imposed with the four selected variables on NO absorption efficiency. Table S2 shows the absorption efficiency of nitric oxide under various parameter values.

Results of variance analysis of second-order formula on nitric oxide absorption efficiency are shown by Table S2. Whether the model term is significant depends on the P-value. The model term is significant by P-value below 0.05, and it is not significant when P value is more than 0.10. The f-value could explain the distribution of experimental NO removal efficiency around the predicted data by the model [36,37].

It can be seen from Table S2 that the model is very significant (P=0.0106) and is reasonable, which is in good agreement with the experimental results. Besides, we could find that three linear terms (temperature, SE concentration, $Fe^{II}EDTA$ concentration) and one quadratic terms (pH) were significant, but the interactive terms were not significant.

Here, the 2D profile was analyzed to demonstrate the variation of dependent variable with independent variable vividly, and the mutual effect of these variables on nitric oxide absorption efficiency could be explained [38]. From Fig. 9, it can be found that NO removal efficiency increased and then decreased with pH value increasing from 4.0 to 12.0. NO removal efficiency decreased as temperature increased from 25 °C to 45 °C. High concentration of SE and $Fe^{II}EDTA$ was conducive to NO removal.

8. Nitric Oxide Absorption Kinetics

The absorption rate of insoluble NO in water was mainly controlled by the chemical reaction in the air-water interface, in which NO was quickly captured through Eq. (1) [39]. The absorption rate of NO could be obtained by Eq. (14).

$$r_{NO}=k_{m,n}C^{m}_{NO,i}C^{n}_{Fe^{II}EDTA} \quad (14)$$

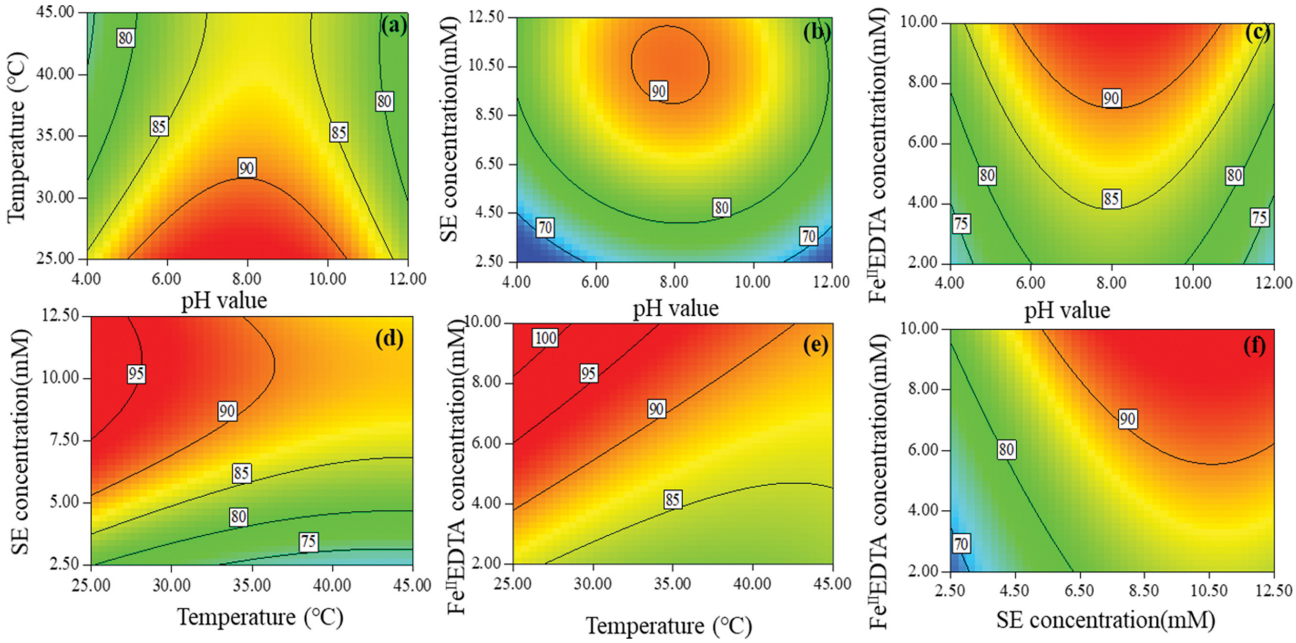

Fig. 9. RSM 2D contour profile of nitric oxide absorption efficiency with the function of pH value and temperature (a); pH and SE concentration (b); pH and $Fe^{II}EDTA$ concentration (c); temperature and SE concentration (d); temperature and $Fe^{II}EDTA$ concentration (e); SE concentration and $Fe^{II}EDTA$ concentration (f).

where $C_{NO,i}$ (mol/L) and $C_{Fe^{II}EDTA}$ (mol/L) are the interface concentration of nitric oxide and $Fe^{II}EDTA$ concentration in solution, respectively; m, n stand for the reactive order, respectively. $k_{m,n}$ is for reaction rate constant. Moreover, the nitric oxide capture by $Fe^{II}EDTA$ in bubbling device was demonstrated to be a pseudo-first-order with $Fe^{II}EDTA$ (n≈1) and a pseudo-second-order with nitric oxide (m≈2), as illustrated by Chu et al. [39] and Wang [40].

Nitric oxide absorption is a mass transfer process in which nitric oxide diffuses from the gas body to the gas-liquid interface and then enters the liquid body. Whitman's double film theory is widely used for explaining the two-phase mass transfer theory, in which the mass transfer rate equation is obtained:

$$N_{NO}=k_{NO,G}(p_{NO,G}-p_{NO,i})=E_f k_{NO,L}(C_{NO,i}-C_{NO,L}) \tag{15}$$

where N_{NO} is the mass transfer rate of nitric oxide, mol/(m^2·s); $p_{NO,G}-p_{NO,i}$ is the differential pressure of nitric oxide between the gas phase bulk and the interface, Pa; $k_{NO,G}$ is the gas phase mass transfer coefficient, mol/(s·m^2·Pa); $C_{NO,i}-C_{NO,L}$ is the differential concentration of nitric oxide between the interface and the liquid phase bulk, mol/L; E_f is enhancement factor; $k_{NO,L}$ stands for liquid mass transfer coefficient, m/s.

The absorption rate of nitric oxide was calculated by the mass balance:

$$N_{NO}=\frac{\overline{\eta}_{AE}C_{NO,in}Q_G}{60{,}000M_{NO}\alpha_{NO}V} \tag{16}$$

where $\overline{\eta}_{AE}$ is the average nitric oxide absorption efficiency, %; α_{NO} is the specific interfacial area, m^{-1}; $C_{NO,in}$ is the nitric oxide inlet concentration, mg/m^3; M_{NO} is nitric oxide molecular weight, g/mol; Q_G is the flue gas velocity, mL/min; V is the solution volume of the reactor, mL.

Based on the mass transfer rate equation and Henry's law, the interface concentration of NO can be obtained as:

$$C_{NO,i}=H_{NO}\left(p_{NO,G}-\frac{N_{NO}}{k_{NO,G}}\right) \tag{17}$$

$$C_{NO,i}=H_{NO}p_{NO,i} \tag{18}$$

$$p_{NO,i}=p_{NO,G}-\frac{N_{NO}}{k_{NO,G}} \tag{19}$$

$$H_{NO}\approx\frac{\rho_S}{EM_S} \tag{20}$$

where ρ_S is the density of H_2O, kg/m^3; E is Henry coefficient of nitric oxide, kPa, referring to related chemical engineering books; M_S is the molar mass of H_2O, g/mol; H_{NO} is the solubility index of nitric oxide, mol/(L·Pa).

Because nitric oxide is difficult to dissolve in solution, its concentration in the main body of the liquid phase is supposed to be zero ($C_{NO,L}$=0). The enhancement factor E_f is given by Eq. (21).

$$E_f=\frac{N_{NO}}{k_{NO,L}\cdot C_{NO,i}} \tag{21}$$

Based on the previous reports [39], the reaction rate of NO absorption by $Fe^{II}EDTA$ is quite fast. The reaction rate constant was gained through combination of traditional kinetic rate formula with the mass transfer rate formula.

$$k_{m,n}=\frac{N_{NO}^2}{\frac{2}{m}D_{NO}C_{NO,i}^m C_{Fe^{II}EDTA}^n} \tag{22}$$

To calculate the above parameters, the related calculation procedures of mass transfer parameters including $k_{NO,G}$, $k_{NO,L}$, α_{NO} are shown in the Text S4.

Here, the chosen experiment parameters for kinetic calculation are: temperature, 25 °C; atmospheric pressure; Q_G, 0.4 L/min; absorbent volume V, 500 mL; pH 8.0; $C_{Fe^{II}EDTA}$=0-0.016 M; nitric oxide concentration, 500 ppm (670 mg/m^3).

Based on the selected experiment parameters and the dynamics analysis, the value of $H_{NO,L}$, $D_{NO,L}$, $D_{NO,G}$, $k_{NO,L}$, $k_{NO,G}$, and a are shown in Table 2.

According to Dual-mode theory, the overall mass transfer resistance ($1/K_{NO,G}$) is obtained by the resistances sum of gas - film ($1/k_G$) and aqueous - film ($1/k_L$).

$$\frac{1}{K_{NO,G}}=\frac{1}{k_{NO,G}}+\frac{1}{EH_{NO}k_{NO,L}} \tag{23}$$

Table 3 implies that the mass transfer kinetics of different $Fe^{II}EDTA$ processes in NO removal was calculated. Compared with other $Fe^{II}EDTA$ systems, the addition of SE increased the NO flux (N_{NO}) by 2-5 times, significantly boosted the total mass transfer coefficients ($K_{NO,G}$), and enhanced factor (E_f). For instance, as SE concentration increased from 0 to 0.02 M, the NO flux and E_f increased from 8.24×10^{-7} to 2.04×10^{-6} mol/(m^2·s) and from 21.99 to 54.72, respectively. As $Fe^{II}EDTA$ concentration increased from 0.002 M to 0.016 M, the N_{NO} and E_f increased from 1.67×10^{-6} to 2.1×10^{-6} mol/(m^2·s) and from 44.87 to 57.40, respectively (Table 3). The results demonstrate that the influence of chemical reactions on mass transfer and absorption increased, while the resistance of liquid film decreased.

To distinguish the control mode of mass transfer, gaseous and liquid film resistances were compared. If $1/k_G$ was close to $1/K_G$, the absorption was governed by gaseous film; if the value of K_G/k_G was lower than 0.1, the transfer was governed by the liquid-phase [41]. As observed in Table 3, K_G/k_G was below 0.1, suggesting that the nitric oxide removal was still governed by the liquid film, though fast chemical reactions could promote the mass transfer coefficient of the liquid phase. Thus, the rate of nitric oxide removal was pri-

Table 2. Physical and mass transfer parameters of NO

Parameters	$H_{NO,L}$ mol·m^{-3}·Pa^{-1}	$D_{NO,L}$ m^2·s^{-1}	$D_{NO,G}$ m^2·s^{-1}	$k_{NO,L}$ m·s^{-1}	$k_{NO,G}$ mol/(s·m^2·Pa)	α m^{-1}
Value	1.91×10^{-5}	2.62×10^{-9}	8.99×10^{-2}	3.93×10^{-5}	7.91×10^{-6}	134.66

Table 3. Mass transfer reaction kinetics parameters of NO absorption

C_{SE} mol/L	$C_{Fe^{II}EDTA}$ mol/L	$\overline{\eta}_{AE}$ %	N_{NO} mol/(m^2·s)	$k_{m,n}$ L·mol^{-1}·s^{-1}	E_f	$K_{NO,G}$ mol/(s·m^2·Pa)	$K_{NO,G}/k_{NO,G}$
0	0.004	37.25	8.24×10^{-7}	71,285.76	21.99	1.65×10^{-8}	0.002083
0.0025	0.004	60.24	1.33×10^{-6}	18,6913.1	35.61	2.66×10^{-8}	0.003368
0.005	0.004	84.57	1.87×10^{-6}	36,9393.2	50.06	3.74×10^{-8}	0.004729
0.01	0.004	90.63	2.00×10^{-6}	42,4517.8	53.67	4.01×10^{-8}	0.005067
0.02	0.004	92.37	2.04×10^{-6}	44,1061.1	54.72	4.09×10^{-8}	0.005165
0.005	0.002	75.83	1.67×10^{-6}	59,3392.3	44.87	3.35×10^{-8}	0.00424
0.005	0.004	84.57	1.87×10^{-6}	36,9393.2	50.06	3.74×10^{-8}	0.004729
0.005	0.008	94.39	2.09×10^{-6}	23,0333.7	55.91	4.17×10^{-8}	0.005278
0.005	0.016	96.9	2.14×10^{-6}	12,1407.7	57.40	4.28×10^{-8}	0.005418

Table 4. Comparison of $Fe^{II}EDTA$ methods on cost (the details of the experimental conditions could be obtained from respective references)

Reference	Absorbent	NO removal efficiency	Absorbent cost[a] $Fe^{II}EDTA$ (¥4,373/kmol)	Cost of 1 ton absorbent (¥)
[12]	Na_2SO_3 (0.25M)+$Fe^{II}EDTA$ (0.01 M)	about 80%	Na_2SO_3 (¥4,000/ton)	¥126+¥43.7=¥169.7
[42]	Na_2SO_3 (0.03 M)+$Fe^{II}EDTA$ (0.01M) +activated carbon (20 g in 500 mL)	90.8%	activated carbon (¥3,200/ton)	¥17.9+¥43.7+¥128=¥189.6
[43]	Mn (0.1 M)+$Fe^{II}EDTA$ (0.003 M)	b	Mn (¥25,000/ton)	¥137.5+¥13.1=¥150.6
[44]	Zn (0.08 M)+$Fe^{II}EDTA$ (0.05 M)	85%	Zn (¥26,000/ton)	¥135.2+¥219.1=¥354.3
[18]	Fe (15 g in 75 mL)+$Fe^{II}EDTA$ (0.02 M)	90.6	Fe (¥4,500/ton)	¥899.6+¥87.7=¥987.3
[15]	$(NH_4)_2SO_3$ (0.1 M)+$Fe^{II}EDTA$ (0.02 M)	80%	$(NH_4)_2SO_3$ (¥3,800/ton)	¥35.9+¥87.7=¥123.6
[45]	Urea (5 wt%)+$Fe^{II}EDTA$ (0.02 M)	78%	Urea (¥2,790/ton)	¥139.5+¥87.7=¥227.2
[46]	VC (0.005 M)+$Fe^{II}EDTA$ (0.004 M)	89%	VC (¥35,000/ton)	¥30.8+¥17.5=¥48.3
here	SE (0.005 M)+$Fe^{II}EDTA$ (0.004 M)	85%	SE ((¥17,000/ton)	¥16.8+¥17.5=¥34.3

[a]Obtained by the Alibaba website

[b]Excellent removal efficiency, and specific value was not given.

marily correlated with gaseous-liquid interface area and liquid film resistance. Increasing the gas-liquid contact area and decreasing the thickness of the liquid resistance can remarkably promote the NO removal process.

9. Technology Analysis

To highlight the advantages of $Fe^{II}EDTA$ and SE system over other $Fe^{II}EDTA$ process, the NO removal in different $Fe^{II}EDTA$ system was contrasted with respect to nitric oxide absorption performance, absorption solution cost, and absorbent disposal. It is difficult to compare the NO removal efficiency of different systems because of the dissimilarities in reaction conditions used by different teams. In general, every literature reporting $Fe^{II}EDTA$ denitrification claimed that their NO removal efficiencies were efficient and excellent. However, price and disposal of absorption solution have a significant impact on practical application. Based on the data from the Alibaba website, the prices of industrial $Fe^{II}EDTA$ and other reducing agents are shown in Table 4. The cost of 1 ton absorbent with respective concentration obtaining the listed NO removal efficiency were calculated, finding that the cost of $Fe^{II}EDTA$ combined with SE system is lowest.

From the point of disposal of absorption solution and operability, when SO_3^{2-} is combined with $Fe^{II}EDTA$ for nitric oxide absorption, the generated by-product N-S compounds are hard to recycle. When reductive metal powder like Fe and Zn is used as combination agent of $Fe^{II}EDTA$, the absorption equipment is easily blocked up by produced precipitation. Here when it comes to SE, NO is mainly transformed into $Fe^{II}EDTA$-NO, then $Fe^{II}EDTA$-NO is desorbed to $Fe^{II}EDTA$ for continued capturing NO. After SE inactivation, $Fe^{II}EDTA$-NO also was slowly oxidized to $Fe^{III}EDTA$, nitrate and nitrite. So the remarkable advantage of SE and $Fe^{II}EDTA$ is that NO and other related products can be recovered, achieving the purpose of turning waste into wealth. Therefore, with respect to economy and operation, SE and $Fe^{II}EDTA$ system can show great advantages.

CONCLUSION

We proposed a novel complexation denitrification technology by $Fe^{II}EDTA$ combined with SE, which can quickly reduce $Fe^{III}EDTA$ to $Fe^{II}EDTA$ and keep $Fe^{II}EDTA$ activity for a long time in air to greatly improve NO absorption by $Fe^{II}EDTA$. With respect to economic cost and operation, SE and $Fe^{II}EDTA$ system can bring more significant superiority than other complexation technologies. Nitric oxide removal efficiency increased with $Fe^{II}EDTA$ or SE concentration increasing, and weak alkalinity (about pH 8.0) and low temperature are beneficial to nitric oxide absorption. As the NO or O_2 concentration increased, the NO removal efficiency continually decreased, while as SO_2 concentration increased, the NO removal

efficiency increased first and then decreased. However, pH and temperature hardly affect the nitric oxide removal efficiency at $Fe^{II}EDTA$ with high concentration. In addition, the kinetic research indicated that NO absorption by mixed $Fe^{II}EDTA$ and SE was more effective, mainly manifested in increasing the reaction rate, reducing total mass transfer resistance and enlarging the NO flux. The absorption process is controlled by the liquid film.

ACKNOWLEDGEMENTS

The project was supported by Jiangxi Natural Science Foundation of China (No. 20212BAB213004).

SUPPORTING INFORMATION

Additional information as noted in the text. This information is available via the Internet at http://www.springer.com/chemistry/journal/11814.

REFERENCES

1. Z. Zhang, S. Zhou, H. Xi and M. Shreka, *Fuel*, **288**, 119709 (2021).
2. Z. Rahman, X. Wang, J. Zhang, J. Baleta, M. Vujanović and H. Tan, *J. Energy Inst.*, **94**, 263 (2021).
3. M. Zhu, Q. Shao, Y. Pi, J. Guo, B. Huang, Y. Qian and X. Huang, *Small*, **13**, 1701295 (2017).
4. H. Hu, X. Fan, X. Gong, R. Zhao and D. Wang, *Chem. Eng. Process.,* **166**, 108466 (2021).
5. M. Zhu, Q. Shao, Y. Qian and X. Huang, *Nano Energy*, **56**, 330 (2019).
6. F. He, X. Zhu, X. Chen and J. Ding, *Chinese J. Chem. Eng.*, **28**, 2918 (2020).
7. T. Zhu, J. Ding, Q. Shao, Y. Qian and X. Huang, *ChemCatChem*, **11**, 689 (2019).
8. W. J. Cai, Z. P. Tang and J. W. Li, *Fuel Process. Technol.*, **140**, 82 (2015).
9. W. Jiang, Q. Xu and X. Wei, *J. Hazard. Mater.*, **374**, 50 (2019).
10. S. Cheon, S. H. Kim, H. C. Yoon and J.-I. Han, *Energy Fuel*, **34**, 9940 (2020).
11. S. Liu, Z. Liu, J. Yang, Y. Sun, L.-c. Nengzi, L. Chen and Y. Yang, *Fuel*, **289**, 119936 (2021).
12. E. Sada, H. Kumazawa and Y. Takada, *Ind. Eng. Chem. Fundam.*, **23**, 60 (1984).
13. S. G. Chang, D. Littlejohn and S. Lynn, *Environ. Sci. Technol.*, **17**, 649 (1983).
14. S. Wang, Z. Qi, Z. Gu, Z. Wang and Z. Ping, *J. Energy Inst.*, **90**, 2528 (2016).
15. B. Yan, J. Yang, M. Guo, G. Chen, Z. Li and S. Ma, *J. Ind. Eng. Chem.*, **20**, 2528 (2014).
16. X. Yang, L. Yang, L. Dong, X. Long and W. Yuan, *Energy Fuel*, **25**, 4248 (2015).
17. K. Xiang, H. Liu, B. Yang, C. Zhang, S. Yang, Z. Liu, C. Liu, X. Xie, L. Chai and X. Min, *Environ. Sci. Pollut. R.*, **23**, 8113 (2016).
18. M. Lefan, T. Zhiquan and Z. Junfeng, *J. Air Waste. Manage.*, **54**, 1543 (2004).
19. X. Dong, Z. Yu, J. Zhou, H. Li, X. Wang and M. Chen, *J. Chem. Technol. Biot.*, **89**, 111 (2013).
20. X. Zhu, F. He, M. Xia, H. Liu and J. Ding, *RSC Adv.*, **9**, 24386 (2019).
21. A. E. Harvey, J. A. Smart and E. S. Amis, *Anal. Chem.*, **27**, 26 (1955).
22. F. He, X. Deng and M. Chen, *Fuel*, **199**, 523 (2017).
23. Chinese Health Ministry, National Food Safety Standard, GB 5009.33 (2010).
24. S. Seibig and R. van Eldik, *Inorg. Chem.*, **36**, 4115 (1997).
25. J. Chen, C. Lin, M. Zhang, T. Jin and Y. Qian, *ChemElectroChem*, **7**, 3311 (2020).
26. A. Bendich, L. J. Machlin, O. Scandurra, G. W. Burton and D. D. M. Wayner, *Adv. Free Radical Bio. Med.*, **2**, 419 (1986).
27. T. T. Suchecki, E. Sada and H. Kumazawa, *Ind. Eng. Chem. Res.*, **30**, 2201 (1991).
28. F. He, X. Zhu, X. Chen and J. Ding, *Asia-Pac. J. Chem. Eng.*, **15**, e2397 (2020).
29. F. He, X. Zhu, X. Chen, Y. Qian and J. Ding, *J. Chem. Technol. Biot.*, **95**, 1392 (2020).
30. F. He, X. Deng and M. Chen, *Fuel*, **199**, 523 (2017).
31. S.-H. Zhang, W. Li, C.-Z. Wu, H. Chen and Y. Shi, *Appl. Microbiol. Biotechnol.*, **76**, 1181 (2007).
32. N. Li, Y. Zhang, Y. Li, M. Chen, X. Dong and J. Zhou, *J. Chem. Technol. Biotechnol.*, **88**, 311 (2013).
33. S. G. Chang, D. Littlejohn and S. Lynn, *Environ. Sci. Technol.*, **17**, 649 (1983).
34. W. Weisweiler, R. Blumhofer and T. Westermann, *Chem. Eng. Process.*, **20**, 155 (1986).
35. F. He, X. Zhu, X. Chen, Y. Qian and J. Ding, *J. Chem. Technol. Biotechnol.*, **95**, 1392 (2020).
36. L. Mohajeri, H. A. Aziz, M. H. Isa and M. A. Zahed, *Bioresour. Technol.*, **101**, 893 (2010).
37. T. Zhu, S. Liu, B. Huang, Q. Shao, M. Wang, F. Li, X. Tan, Y. Pi, S.-C. Weng, B. Huang, Z. Hu, J. Wu, Y. Qian and X. Huang, *Energ. Environ. Sci.*, **14**, 3194 (2021).
38. Y. Wu, S. Zhou, F. Qin, X. Ye and K. Zheng, *J. Hazard. Mater.*, **180**, 456 (2010).
39. T. W. Chien, H. T. Hsueh, B. Y. Chu and H. Chu, *Process. Saf. Environ.*, **87**, 300 (2009).
40. F. Wang, *Research of nitric oxide complexing absorbed by $Fe^{II}EDTA$*, North University of China, Taiyuan (2015).
41. M. Chen, X. Deng and F. He, *Energy Fuel*, **30**, 1183 (2016).
42. H. S. Zhu, Y. P. Mao, X. J. Yang, C. Yu, X. L. Long and W. K. Yuan, *Sep. Purif. Technol.*, **74**, 1 (2010).
43. Y. Duo, X. Wang, J. He, S. Zhang, H. Pan, J. Chen and J. Chen, *Environ. Sci. Pollut. R.*, **26**, 28808 (2019).
44. H. Zhu, Z. Nie, Y. Hu, J. Wang, H. Bai, Y. Li, Q. Guo and C. Wang, *Energy Fuel*, **33**, 8998 (2019).
45. F. He, X. Deng and M. Chen, *Chemosphere*, **168**, 623 (2017).
46. F. He, X. Zhu, X. Chen and J. Ding, *Fuel*, **284**, 119070 (2021).

Supporting Information

Novel NO removal using combined sodium erythorbate and $Fe^{II}EDTA$ system

Lirong Zhong, Feiqiang He†, Beibei Dong, and Jianhua Ding†

Jiangxi Key Laboratory for Mass Spectrometry and Instrumentation, East China University of Technology, Nanchang 330013, P. R. China

(*Received 6 January 2022 • Revised 1 April 2022 • Accepted 24 April 2022*)

S1. The Relation between SE and $Fe^{II}EDTA$.

$Fe^{III}EDTA$ reduction procedure: A 250 mL flask with a pH electrode was set in a heat collection-constant temperature type magnetic stirrer (Fig. S1). 250 mL aqueous $Fe^{III}EDTA$ solution was obtained by blending Na_2EDTA and $NH_4Fe(SO_4)_2{\cdot}12H_2O$ in the flask. Then the solution was separated from the atmospheric oxygen with 3 L min^{-1} continuous N_2 (99.999%) stream. Then, the pH value was adjusted with H_2SO_4 and NaOH solution. The $Fe^{III}EDTA$ reduction was initiated after adding SE into the $Fe^{III}EDTA$ solution with stirring speed of 2,500 r/min. Finally, $Fe^{II}EDTA$ concentration of the solution was measured at specific time intervals.

$Fe^{II}EDTA$ inhibiting oxidation procedure: A 250 mL flask with $Fe^{II}EDTA$ solution was set in a heat collection-constant temperature type magnetic stirrer (Fig. S1). Then, the pH value was adjusted with H_2SO_4 and NaOH solution. Different reducing agent were added into the $Fe^{II}EDTA$ solution with stirring speed of 2,500 r/min. The flask was not stoppered and the solution was directly exposed to air. Finally, $Fe^{II}EDTA$ concentration was measured at specific time intervals.

S2. NO Removal

The absorption plant includes gas distributing system, bubbling reactor, and flue gas analyzer, as illustrated in Fig. S2. Absorption of NO was conducted in the bubbling reactor of 500 mL erlenmeyer flask with atmospheric pressure. Firstly, the ultimate pressure of the gas buffer tank (20 L) was set as 0.1 MPa (gauge pressure). Based on the pressure and volume of gas buffer tank, the volume of the needed NO concentrations (500 ppm) can be informed. Then NO was poured successively into gas buffer tank by adjusting the corresponding rotameter. The needed O_2 concentration was achieved by blending air and N_2. The absorbing liquid was prepared by adding SE into $Fe^{II}EDTA$ solution. The pH value of the mixed absorbent was regulated with NaOH solution and H_2SO_4. The NO absorption was conducted after N_2 flowing through bubbling reactor for cleaning up residual air. Each experimental group of NO removal was run for 40 min, and the data were measured every 4 min. The absorption solution volume was 500 mL, the nitric oxide import concentration was 500 ppm, and the gas flow rate was 0.4 L min^{-1}, Finally, the NO outlet concentration was tested by a

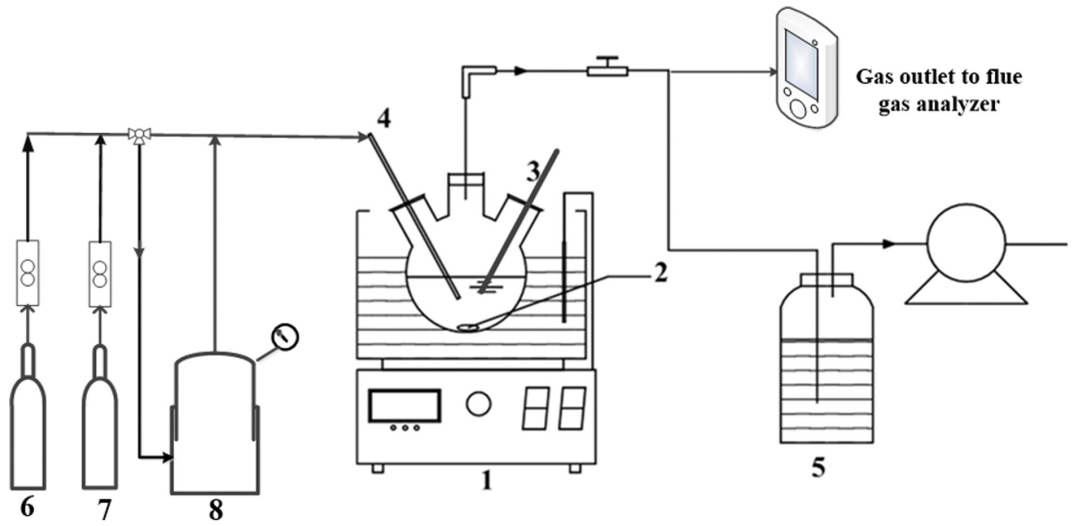

Fig. S1. Experimental apparatus of the relation between SE and $Fe^{II}EDTA$.

1. Heat collection-constant temperature type magnetic stirrer
2. Magnetic stirrer
3. The pH electrode
4. Nitrogen or mixture of NO and N_2 inlet
5. Buffer tank
6. N_2 cylinder
7. NO cylinder
8. Mixture of NO and N_2 cylinder

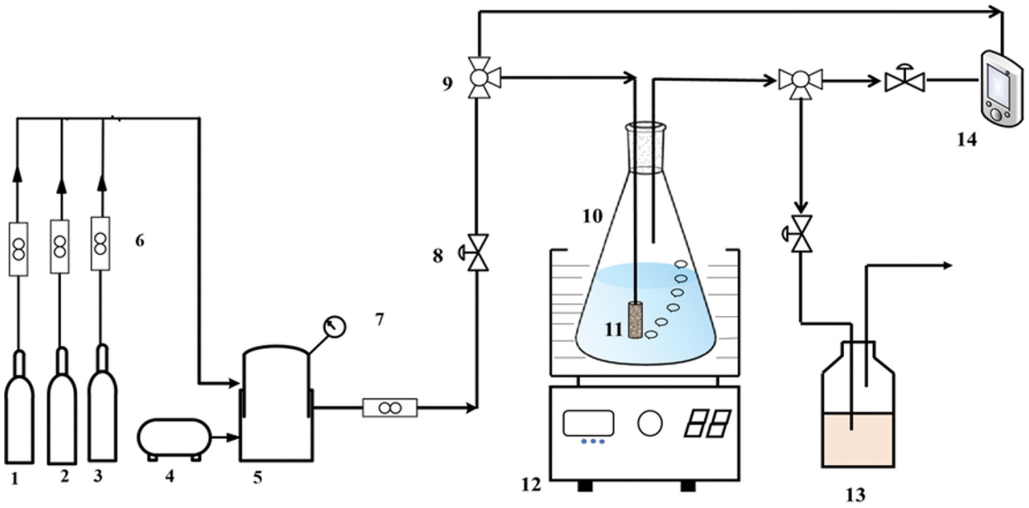

Fig. S2. Experimental apparatus for NO removal by mixed $Fe^{II}EDTA$ and SE system.

1. NO cylinder
2. SO_2 cylinder
3. N_2 cylinder
4. Air compressor
5. Mixed cylinder
6. Gas rotameter
7. Piezometer
8. Two-port valve
9. Three-port valve
10. Absorption bottle
11. Metal aerator
12. Thermostatic water bath
13. Waste gas absorption bottle
14. Flue gas analyzer

Table S1. Codes and levels of experiment factors by CCD

Influencing factors of NO absorption	Value level				
	$-\alpha$	−1	0	1	α
pH value, X_1	4.0	6.0	8.0	10.0	12.0
Temperature (°C), X_2	25	30	35	40	45
SE concentration (mM), X_3	2.5	5	7.5	10	12.5
$Fe^{II}EDTA$ concentration (mM), X_4	2	4	6	8	10

fixed time span.

S3. Experimental Design for RSM Analysis

RSM is often adept in data modeling by experiment design. In addition, it has been widely employed in investigating different types of emulation optimizing, parameter fitting and observing design in science and engineering. In order to optimize NO absorption with mixed $Fe^{II}EDTA$ and SE system, four variables were used including pH value, temperature, SE concentration, and $Fe^{II}EDTA$ concentration by the central composite design (CCD) experiment by RSM, and they were separately labelled as X_1, X_2, X_3, X_4. The code value of 1, 0, and −1 stands for the high, medium, and low levels of independent variables, respectively. Besides, the spots sign as $-\alpha$ and $+\alpha$ can be used to verify this model of this paper (Table S1).

Firstly, the numbers of experiments can be based on Eq. (S1).

$$N=2^k+2k+C_0 \quad \text{(S1)}$$

Where N stands for number of trials; k=4 (number of variables); and C_0=6 in this work.

So the experimental designs were conducted by CCD with 30 trials in Table S2. In this way, the complexity of the experiment can be reduced and less errors can be produced, and the relationship between fractional factorial design and incomplete block design can be established.

Table S2. Experimental designs and experimental values obtained

Serial number	Influence factors				NO removal efficiency
	X_1	X_2	X_3	X_4	Experimental value
1	6	40	5	4	80.37
2	8	35	7.5	6	88.43
3	6	30	10	4	89.54
4	8	35	7.5	6	88.32
5	10	40	10	8	88.92
6	8	35	7.5	6	88.67
7	8	35	7.5	6	88.53
8	6	40	10	4	82.75
9	6	40	10	8	86.65
10	8	45	7.5	6	84.33
11	10	40	10	4	84.56
12	8	25	7.5	6	90.37
13	4	35	7.5	6	76.52
14	8	35	7.5	6	87.57
15	8	35	7.5	2	76.83
16	10	40	5	4	80.21
17	10	40	5	8	84.53
18	12	35	7.5	6	72.57
19	10	30	5	4	84.21
20	8	35	12.5	6	93.12
21	6	40	5	8	81.03
22	10	30	10	4	87.83
23	8	35	7.5	6	87.92
24	8	35	2.5	6	64.35
25	6	30	5	4	80.77
26	6	30	5	8	90.12
27	10	30	5	8	90.21
28	10	30	10	8	93.57
29	6	30	10	8	93.72
30	8	35	7.5	10	93.58

Table S3. ANOVA result of CCD

Source	Sum of squares	df	Mean square	f-Value	p-Value (Prob>F)
Model	983.22	14	70.23	3.52	0.0106
X_1-pH value	0.059	1	0.059	0.00296	0.9574
X_2-temperature	117.17	1	117.17	5.87	0.0285
X_3-urea conc.	365.27	1	365.27	18.3	0.0007
X_4-Fe^{II}EDTA conc.	216.06	1	216.06	10.83	0.005
X_1X_2	2.07	1	2.07	0.1	0.7521
X_1X_3	1.35	1	1.35	0.068	0.7982
X_1X_4	0.34	1	0.34	0.017	0.898
X_2X_3	0.43	1	0.43	0.021	0.8858
X_2X_4	9.05	1	9.05	0.45	0.511
X_3X_4	0.29	1	0.29	0.014	0.9058
X_1^2	190.55	1	190.55	9.55	0.0075
X_2^2	8.77	1	8.77	0.44	0.5174
X_3^2	69.19	1	69.19	3.47	0.0823
X_4^2	0.024	1	0.024	0.0012	0.9731
Residual	299.33	15	19.96		
Lack of fit	298.47	10	29.85	172.97	0.0275
Pure error	0.86	5	0.17		
Cor total	1,282.56	29			

The quadratic equation Eq. (S2) can be employed for fitting the response value of independent variable.

$$Y=\beta_0+\sum_{i=1}^{k}\beta_i x_i+\sum_{i=1}^{k}\beta_{ii}x_i^2+\sum_{1\ll i\ll j}^{k}\beta_{ij}x_i x_j \tag{S2}$$

where Y stands for the response value; β_{ij} and β_{ii} stand for interaction coefficient and second-order migration term coefficients, respectively; x_i and x_j are coding values of variables; β_0, and β_i stand for coefficients of deviation term and linear migration term, respectively.

The NO removal efficiency was measured by different the experimental conditions given by the system Design-Expert statistical software to investigate the influence imposed with the four selected variables on NO absorption efficiency. Table S2 shows the absorption efficiency of nitric oxide under various parameter values.

S4. Mass Transfer Parameters

According to the previous research [1], the gas phase and liquid mass transfer coefficients, $k_{NO,G}$ and $k_{NO,L}$ could be calculated via Eqs. (S3) and (S4).

$$k_{NO,L}=k_{CO_2,L}\left(\frac{D_{NO-H_2O}}{D_{CO_2-H_2O}}\right)^{\lambda} \tag{S3}$$

$$k_{NO,G}=k_{CO_2,G}\left(\frac{D_{NO-N_2}}{D_{CO_2-N_2}}\right)^{\lambda} \tag{S4}$$

$$\alpha_{NO}=\alpha_{CO_2} \tag{S5}$$

Where λ=0.5-1. But in a bubbling reactor, it can be considered equal to 1 [2]. $k_{CO_2,L}$, m/s and $k_{CO_2,G}$, mol/(m^2·Pa·s) are the mass transfer coefficients of CO_2 in gas and liquid phase, respectively; D_{NO-N_2} and $D_{CO_2-N_2}$ are respectively gas diffusion coefficients of NO and CO_2 in N_2, m^2/s; D_{NO-H_2O} and $D_{CO_2-H_2O}$ are respectively liquid diffusion coefficients of NO and CO_2 in H_2O, m^2/s; α_{NO} and α_{CO_2} are the specific interfacial areas of NO and CO_2, respectively, m^{-1}.

The gas-liquid mass transfer parameters $k_{CO_2,L}$, $k_{CO_2,G}$, α_{CO_2} of CO_2 in the reactor can be determined by using the classical chemical absorption methods and Danckwerts plot theory. The detailed steps can be seen related literatures [3,4].

Through consulting chemical industry manual and related reports, D_{NO-N_2} and $D_{CO_2-N_2}$ could be obtained by Champman-Enskog equation.

$$D_{AB}=0.00266\frac{T^{1.5}}{PM_{AB}^{0.5}\Omega_D\sigma_{AB}^2} \tag{S6}$$

Where T is absolute temperature, K; P is pressure, atm. M_{AB} is relative molecular mass, and $M_{AB}=2(1/M_A+1/M_B)^{-1}$; σ_{AB} is characteristic length, and $\sigma_{AB}=\sigma_A/2+\sigma_B/2$; Ω_D is diffusion collision integral and could be obtained by Eq. (S7).

$$\Omega_D=\frac{A}{(T^*)^B}+\frac{C}{\exp(DT^*)}+\frac{E}{\exp(FT^*)}+\frac{G}{\exp(HT^*)} \tag{S7}$$

Where A=1.06036, B=0.15610, C=0.19300, D=0.47635, E=1.03587, F=1.52996, G=1.76474, H=3.89411.

$$T^*=\frac{k_BT}{\varepsilon_{AB}}=\frac{T}{\sqrt{\frac{\varepsilon_A\varepsilon_B}{k_Bk_B}}} \tag{S8}$$

Where k_B is Boltzmann constant; ε_{AB} is Characteristic energy. The relevant parameters can be seen Table S4.

D_{NO-H_2O} and $D_{CO_2-H_2O}$ could be obtained by Wilke-Chang equation [5].

$$D_{AB}=7.4\times10^{-12}\frac{(\Phi_BM_B)^{0.5}T}{\mu_BV_{bA}^{0.6}} \tag{S9}$$

Table S4. Gas characteristic parameters

Parameter	NO	N_2	CO_2
σ (Å)	3.492	3.798	3.941
ε/k_B (K)	116.7	71.4	195.2

Where Φ_B is association factor of solvent B, which is 2.6 for H_2O; M_B is relative molecular mass of B; μ_B is the viscosity of B, cP; V_{bA} is the molar volume of gas, which is 23.6 and 34.0 for NO and CO_2, cm^3/mol.

REFERENCES

1. E. Sada, H. Kumazawa, I. Kudo and T. Kondo, *Ind. Eng. Chem. Process Des. Dev.*, **19**, 377 (1980).
2. H. Hikita, S. Asai and T. Takatsuka, *Chem. Eng. J.*, **11**, 131 (1976).
3. R. Hao, X. Mao, Z. Wang, Y. Zhao, T. Wang, Z. Sun, B. Yuan and Y. Li, *J. Hazard. Mater.*, **368**, 234 (2019).
4. Q. Ye, *Gaseous mercury absorption from simulated flue gas*, Zhejiang University, Hangzhou (2006).
5. C. R. Wilke and P. Chang, *AIChE J.*, **1**, 264 (1955).